electronics

MDPI

Article

Fine-Tuned Aggregation Control in Perylene Diimide-Based Organic Solar Cells via a Mixed-Acceptor Strategy Using Planar and Twisted Acceptors

Hyeongjin Hwang [1,*] and Hansol Lee [2,*]

[1] Department of Chemical and Biological Engineering, Chungwoon University, Incheon 22100, Republic of Korea
[2] School of Chemical, Biological and Battery Engineering, Gachon University, Seongnam 13120, Republic of Korea
* Correspondence: hjhwang@chungwoon.ac.kr (H.H.); hlee22@gachon.ac.kr (H.L.)

Abstract

In bulk heterojunction (BHJ) organic solar cells (OSCs) employing perylene diimide (PDI)-based non-fullerene acceptors, excessive intermolecular interactions among PDI units lead to severe aggregation and pronounced donor–acceptor phase separation, both of which critically limit device performance. To address these issues, numerous structurally engineered PDI derivatives have been developed. In particular, twisted multi-PDI architectures designed to suppress intermolecular aggregation have shown improved morphological control; however, such twisted structures are often highly amorphous, which reduces electron-transport efficiency and constrains OSC performance. In this work, we introduce a mixed-acceptor strategy combining a twisted PDI dimer (SF-PDI_2) with a planar monomeric PDI (m-PDI) to balance aggregation and morphological uniformity. Ternary blend OSCs consisting of PTB7-Th as the donor and these two PDI acceptors exhibit systematic performance variations depending on their relative ratios. At the optimized composition (SF-PDI_2:m-PDI = 90:10 by weight), the device outperforms single-acceptor systems, which is attributed to controlled aggregation arising from the complementary structural features of the two PDI acceptors. This study demonstrates that combining mixed PDI acceptors with similar molecular moieties enables precise control of aggregation, improving both morphology and photovoltaic performance.

Keywords: non-fullerene acceptors; perylene diimides; molecular aggregation; organic solar cells; blend morphology

Check for updates

Academic Editors: Zhuoran Wang, Wenhao Ran and Elias Stathatos

Received: 23 December 2025
Revised: 13 January 2026
Accepted: 10 February 2026
Published: 2 March 2026

Copyright: © 2026 by the authors. Licensee MDPI, Basel, Switzerland. This article is an open access article distributed under the terms and conditions of the Creative Commons Attribution (CC BY) license.

1. Introduction

Organic solar cells (OSCs) have emerged as promising next-generation photovoltaic technologies owing to their lightweight, various form factors, mechanical flexibility, tunable absorption, and compatibility with solution processing [1–4]. Recent advances in non-fullerene acceptors have significantly improved device efficiency and operational stability, largely driven by molecular design strategies, morphology optimization, and multicomponent device architectures such as ternary bulk heterojunction and layer-by-layer configurations [5–13]. Among non-fullerene acceptors, perylene diimide (PDI) derivatives have attracted considerable attention because of their strong electron affinity, excellent thermal stability, and synthetic tunability, enabling widespread application in organic electronics [9,14–19].

Despite these advantages, many planar monomeric PDI derivatives exhibit strong π–π stacking tendencies due to their highly planar structures, often resulting in excessive aggregation in thin films. Such aggregation typically induces large crystalline domains and poor intermixing with polymer donors, hindering exciton dissociation and consequent charge photogeneration. Previous studies examining planar PDI acceptors have reported poor device performance caused by aggregation-driven phase separation [15,20–22]. Thus, controlling the aggregation behavior of PDI-based acceptors remains one of the central challenges in their use for OSCs.

To address these issues, numerous multi-PDI and twisted PDI structures have been developed [14,21,23–30]. Bay-linked and imide-linked PDI dimers, as well as multi-branched architectures, introduce steric hindrance to suppress long-range aggregation. Among these, spiro-linked PDI dimers such as SF-PDI_2 and SF-iPDI_2 represent unique structural innovations where a rigid spiro-bifluorene core enforces an orthogonal geometry between PDI planes, effectively reducing π–π interactions and yielding smoother, more amorphous films [8,16,22,31,32]. While these twisted structures improve morphological uniformity, their amorphous nature can limit long-range electron transport, resulting in trade-offs between aggregation suppression and electron mobility [5,11,32,33].

In this context, we propose a mixed-acceptor strategy that combines planar and twisted PDI acceptors in ternary blend systems. The mixed-acceptor approach provides an additional degree of control over the aggregation behavior of PDI acceptors, thereby enabling potential improvements in OSC performance beyond what can be achieved with single acceptor formulations [34–36]. To investigate this concept, we employ both a planar monomeric PDI (m-PDI) and a twisted spiro-linked PDI dimer (SF-PDI_2) as electron acceptors in donor polymer:PDI acceptor bulk heterojunction OSCs. These two acceptors exhibit intrinsically contrasting aggregation tendencies: m-PDI tends to form ordered molecular stacking that facilitates electron transport, whereas SF-PDI_2 suppresses excessive crystallization and helps maintain morphological uniformity. To systematically assess the impact of mixing PDI acceptors with complementary aggregation characteristics on the morphology and device performance of OSCs, comprehensive electrical, microscopic, and spectroscopic characterizations were conducted on donor:acceptor blends with varying m-PDI:SF-PDI_2 ratios. As a result, we demonstrate that optimizing the blending ratio between these complementary PDI acceptors enables precise control of aggregation behavior, ultimately leading to maximized device performance.

2. Materials and Methods

2.1. Materials

Poly([2,6′-4,8-di(5-ethylhexylthienyl)benzo[1,2-b;3,3-b]dithiophene]{3-fluoro-2[(2-ethylhexyl)carbonyl]thieno[3,4-b]thiophenediyl}) (PTB7-Th) was purchased from 1-Material Inc. (Dorval, QC, Canada). The PDI-based acceptors, SF-PDI_2 and m-PDI, were synthesized following previously reported procedures with minor modifications [8,16,31,32]. All chemicals, including chlorobenzene (CB) used as the solvent for preparing and coating the donor:acceptor blend solutions and the reagents required for the fabrication of the zinc oxide (ZnO) interlayer, were purchased from Sigma Aldrich (Burlington, MA, USA) and used as received without further purification. The hole transport layer material, MoO_3, was purchased from Tokyo Chemical Industry (Tokyo, Japan).

2.2. Fabrication of Devices

Organic solar cells were fabricated in an inverted device architecture of ITO/ZnO (50 nm)/active layer (PTB7-Th:mixed-PDI blend)/MoO_3 (3 nm)/Ag (80 nm). ITO-coated glass substrates were cleaned by sequential ultrasonication in detergent solution, distilled

water, acetone, and isopropanol for 15 min each, followed by UV–ozone treatment for 20 min. A ZnO electron-transport layer was deposited by spin coating a ZnO precursor solution onto the substrate at 4000 rpm, followed by thermal annealing at 180 °C for 10 min. The ZnO precursor solution was prepared by dissolving zinc acetate dehydrate, monoethanolamine, and 2-methoxyethanol with stirring for 8 h, following a procedure reported previously [37]. Active layer solutions were prepared in CB at 55 °C, dissolving PTB7-Th at a concentration of 10 mg mL^{-1} and mixed PDI acceptors at a total concentration of 10 mg mL^{-1}. The donor to acceptor weight ratio was fixed at 1:1, as prior studies on PDI acceptor-based OSCs have commonly reported optimal donor to acceptor ratios around this value [27,31,32]. While the relative ratio between the two acceptors within the mixed-PDI acceptor system was varied, the overall donor to total acceptor ratio was intentionally kept constant at 1:1. This design choice was made to more clearly isolate and examine the effects of PDI acceptor mixing on aggregation behavior and blend morphology. For the mixed-PDI acceptor system, four blend ratios of SF-PDI_2 to m-PDI (100:0, 90:10, 80:20, and 0:100) were investigated. The warm solutions were spin-coated onto the ZnO-coated substrates at speeds ranging from 700 to 4000 rpm. After active layer deposition, a 3 nm thick MoO_3 layer and an 80 nm thick Ag electrode were sequentially deposited by thermal evaporation under high vacuum conditions below 4×10^{-6} Torr. Electron-only devices for space-charge-limited current (SCLC) measurements were fabricated with a device configuration of ITO/ZnO/active layer (mixed-acceptor-only)/LiF (6 Å)/Al (80 nm). LiF and Al were deposited by thermal evaporation under the same high vacuum conditions.

2.3. Characterizations

Current density–voltage (*J*-*V*) characteristics of devices were recorded using a Keithley 2400 source meter (Tektronix, Beaverton, OR, USA). Photovoltaic performance of the solar cell devices was measured under AM1.5G illumination at an intensity of 100 mW cm^{-2} generated by an Oriel 1 kW solar simulator, which was calibrated using a certified silicon reference cell (Newport). SCLC measurements of electron-only devices were performed in the dark, and the dark *J*-*V* curves were fitted using the Mott–Gurney law to extract electron mobilities. All electrical measurements were carried out inside a nitrogen-filled glovebox. UV–vis absorption spectra were recorded using a CARY-5000 spectrometer (Varian, Palo Alto, CA, USA). External quantum efficiency (EQE) measurements were obtained using an Oriel IQE-200 system (Newport, Irvine, CA, USA). Atomic force microscopy (AFM) images were obtained using an NX-10 atomic force microscope (Park Systems, Suwon, Republic of Korea) operated in the non-contact mode.

3. Results and Discussion

3.1. Molecular Structure of PDI Acceptors

The molecular structures of the donor and acceptor materials used in this study are shown in Figure 1. PTB7-Th was employed as the donor polymer owing to its broad absorption in the visible region, suitable energy-level alignment, and well-documented performance in various OSC systems. Two structurally distinct PDI acceptors, m-PDI and SF-PDI_2, are also presented. Based on prior reports [8,27,31,32], the highest occupied molecular orbital (HOMO) and lowest unoccupied molecular orbital (LUMO) energy levels of PTB7-Th are reported to be approximately −5.2 and −3.3 eV, respectively, and the HOMO and LUMO energy levels of PDI acceptors vary slightly depending on their molecular structures, but are generally around −6.0 and −3.8 eV, respectively. That is, the LUMO levels of both PDI acceptors are sufficiently lower than that of PTB7-Th, while their HOMO levels are also positioned deeper than the HOMO of PTB7-Th. This favorable energy-level alignment provides adequate driving forces for electron transfer from the donor to the

acceptor and hole transfer from the acceptor to the donor, thereby enabling efficient exciton separation at the donor–acceptor interface.

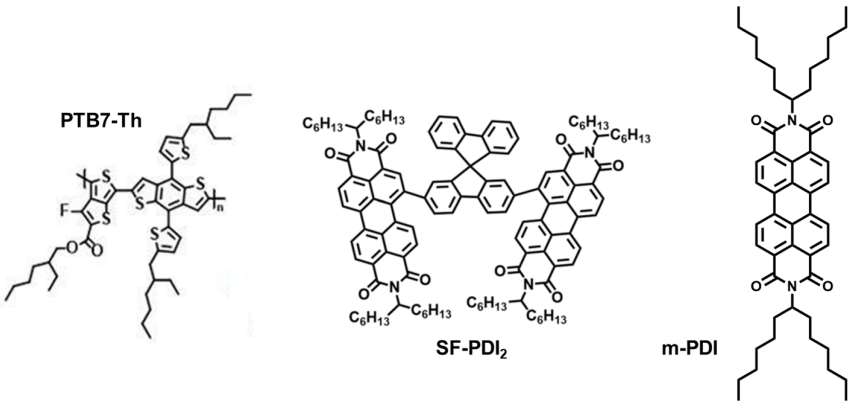

Figure 1. Molecular structures of PTB7-Th, SF-PDI_2, and m-PDI.

The m-PDI acceptor possesses a fully planar conjugated core with symmetric branched alkyl chains at both imide positions. The high planarity of m-PDI promotes strong π–π interactions, leading to persistent intermolecular stacking and pronounced aggregation. Numerous studies have reported that planar PDI derivatives readily form large crystalline domains in thin films, which results in unfavorable phase separation in OSCs [20,22]. Such structural characteristics often limit photocurrent generation due to the reduced interfacial area between the donor and acceptor phases. In contrast, SF-PDI_2 consists of two PDI units connected at the bay positions through a rigid spiro-bifluorene scaffold, which enforces a nearly orthogonal orientation between the two fluorene moieties [16]. This twisted three-dimensional geometry effectively disrupts π–π stacking between adjacent PDI planes and suppresses long-range crystallization, leading to smoother and more amorphous film morphologies. The reduced aggregation behavior of SF-PDI_2 is advantageous for achieving uniform donor–acceptor mixing within the bulk heterojunction [38].

Because planar m-PDI facilitates electron transport through localized aggregation, whereas twisted SF-PDI_2 suppresses excessive stacking and preserves nanoscale morphological uniformity, blending these two acceptors is expected to produce complementary morphological effects. We therefore hypothesized that incorporating a small fraction of m-PDI into an SF-PDI_2-rich matrix would introduce controlled aggregation that enhances electron transport, while the dominant SF-PDI_2 fraction prevents the formation of large crystalline domains. This complementary interaction constitutes the conceptual basis of our mixed-acceptor strategy.

Bulk heterojunction active layers were fabricated using PTB7-Th as the donor and mixtures of SF-PDI_2 and m-PDI as the acceptors. The donor-to-acceptor weight ratio was fixed at 1:1, while the relative weight ratios of the two PDI acceptors were systematically varied (SF-PDI_2:m-PDI = 100:0, 90:10, 80:20, and 0:100), as described in the Materials and Methods section. For convenience, the acceptor mixtures with SF-PDI_2:m-PDI ratios of 100:0, 90:10, 80:20, and 0:100 are hereafter referred to as the "100% SF-PDI_2," "90% SF-PDI_2," "80% SF-PDI_2," and "0% SF-PDI_2" acceptors, respectively. These compositions were selected to examine how the gradual introduction of planar m-PDI influences film morphology and device characteristics. High fractions of m-PDI were expected to intensify aggregation and degrade device performance. Accordingly, SF-PDI_2 was used as the major acceptor component, with m-PDI introduced only in minor amounts. The incorporation of a small amount of m-PDI was anticipated to enhance π–π stacking between PDI molecules within the mixed-acceptor system without significantly compromising the smooth and uniform blend morphology primarily provided by SF-PDI_2. It is worth noting that, given

the high compatibility between m-PDI and SF-PDI$_2$, our system falls into the category of one-donor–two-acceptor alloy-type ternary OSCs [39], where the particular focus of this work lies on finely controlled molecular aggregation within the alloyed PDI acceptor phase.

3.2. Aggregation Behavior of Mixed-Acceptor Systems

The UV–vis absorption spectra of PTB7-Th-only, mixed-PDI-only, and PTB7-Th:mixed-PDI blend films are shown in Figure 2. PTB7-Th exhibits strong absorption in the 500 to 800 nm range, whereas PDI-based acceptors primarily absorb between 400 and 600 nm. The m-PDI-only film (0% SF-PDI$_2$) displays pronounced vibronic shoulder features at 520 to 560 nm, reflecting the ordered aggregation and strong π–π stacking tendency of the planar PDI units [20,40]. In contrast, films containing SF-PDI$_2$ exhibit much smoother absorption features, indicative of their largely amorphous nature with suppressed molecular packing. Notably, even in the 90% SF-PDI$_2$ film, weak shoulder-like features are observed, suggesting that the incorporation of m-PDI induces controlled and moderate aggregation. Such subtle aggregation is expected to promote electron transport pathways while preserving overall film uniformity [41–43]. Absorption features associated with m-PDI induced aggregation are observed not only in mixed-PDI-only films but also in the absorption spectra of PTB7-Th:mixed-PDI blend films.

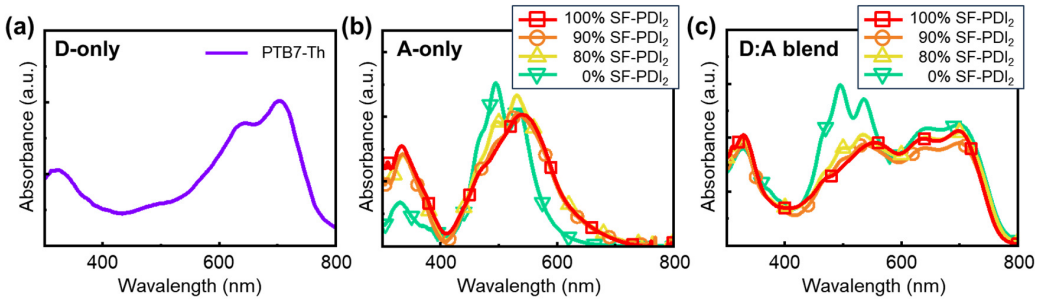

Figure 2. UV–vis absorption spectra of the materials used in this study in the solid film state. (**a**) PTB7-Th-only film. (**b**) Mixed-PDI-only films. (**c**) PTB7-Th:mixed-PDI blend films. The mixed-PDI acceptors have various weight ratios of SF-PDI$_2$:m-PDI, 100:0 (100% SF-PDI$_2$), 90:10 (90% SF-PDI$_2$), 80:20 (80% SF-PDI$_2$), and 0:100 (0% SF-PDI$_2$).

AFM height images of the mixed-PDI-only and PTB7-Th:mixed-PDI blend films (Figure 3) provide direct insight into the morphological evolution as a function of m-PDI content. The pure SF-PDI$_2$ film exhibits a very smooth surface with a root-mean-square (rms) roughness (R_{rms}) of 0.29 nm, consistent with its amorphous character. The introduction of small amounts of m-PDI leads to a gradual increase in R_{rms} for the mixed-PDI-only films, with values of R_{rms} = 0.36 nm and 0.64 nm for the 90% SF-PDI$_2$ and 80% SF-PDI$_2$ films, respectively. These results clearly indicate that the m-PDI induces molecular aggregation, which contributes to increased surface roughness. It is important to note that, although the addition of small amounts of m-PDI leads to the formation of fine scale aggregation of PDI acceptors, it does not result in pronounced crystallization of m-PDI or phase separation between m-PDI and SF-PDI$_2$ within the composition range examined. Similar morphological trends are observed in the PTB7-Th:mixed-PDI blend films. Specifically, the R_{rms} values increase gradually with increasing m-PDI content, reaching 1.43, 1.96, and 2.15 nm for blend films containing 100% SF-PDI$_2$, 90% SF-PDI$_2$, and 80% SF-PDI$_2$ acceptors, respectively, without showing any sign of phase separation or excessively grown m-PDI crystalline domains. These morphological observations are in good agreement with the UV-vis absorption results, supporting the effectiveness of the mixed-PDI strategy in enabling fine control over molecular aggregation in the blend films.

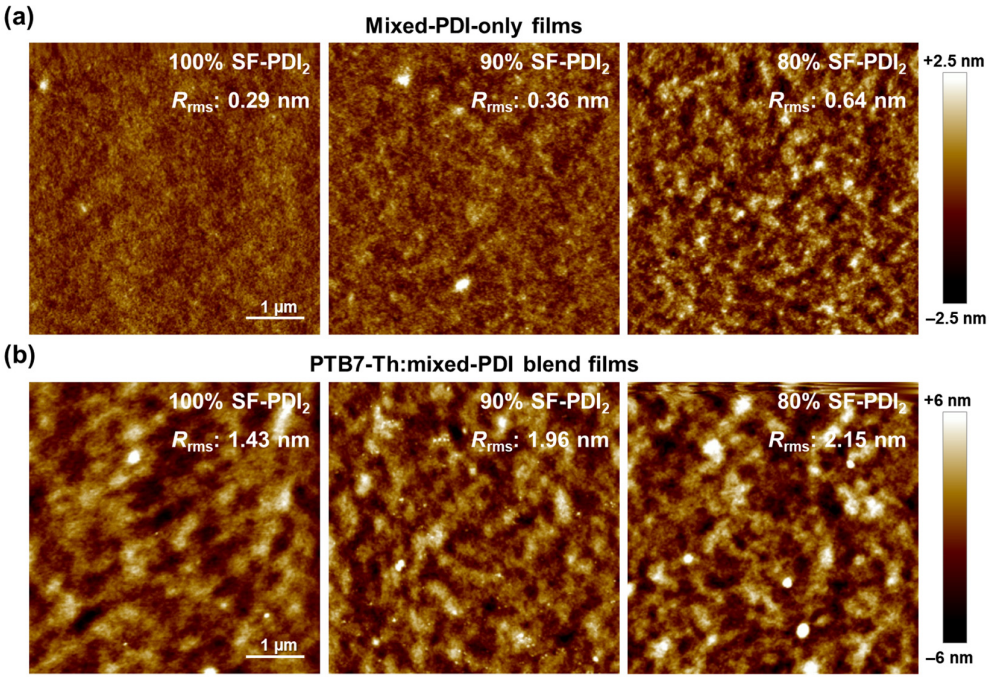

Figure 3. AFM height images of (**a**) mixed-PDI-only films and (**b**) PTB7-Th:mixed-PDI blend films with different SF-PDI$_2$:m-PDI ratios, together with the corresponding rms roughness values. Scale bar: 1 μm.

3.3. Photovoltaic Performance

Figure 4a presents the *J*-*V* characteristics of the OSC devices with various mixed-PDI acceptor compositions measured under AM1.5G one-sun illumination. The corresponding photovoltaic parameters, including short-circuit current density (J_{SC}), open-circuit voltage (V_{OC}), fill factor (FF), and power conversion efficiency (PCE), are summarized in Table 1.

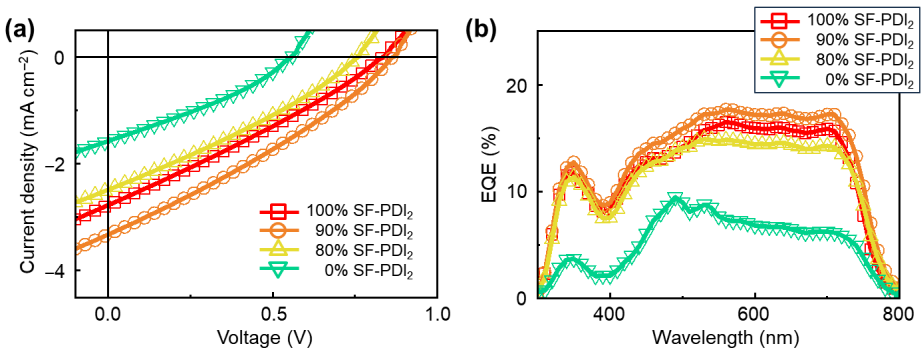

Figure 4. Photovoltaic characteristics of the PTB7-Th:mixed-PDI blend-based OSCs with different SF-PDI$_2$:m-PDI acceptor ratios. (**a**) *J*-*V* characteristics. (**b**) EQE spectra.

Table 1. Photovoltaic parameters of PTB7-Th:mixed-PDI OSC devices measured under AM1.5 one-sun illumination. Values are averaged over at least five devices, with standard deviations in parentheses.

Device	J_{SC}	V_{OC}	FF	PCE
	[mA cm^{-2}]	[V]		[%]
100% SF-PDI$_2$	2.67 (±0.154)	0.830 (±0.027)	0.282 (±0.004)	0.624 (±0.042)
90% SF-PDI$_2$	3.28 (±0.139)	0.845 (±0.050)	0.303 (±0.005)	0.840 (±0.072)
80% SF-PDI$_2$	2.39 (±0.115)	0.773 (±0.012)	0.294 (±0.004)	0.544 (±0.026)
0% SF-PDI$_2$	1.62 (±0.163)	0.567 (±0.012)	0.313 (±0.003)	0.287 (±0.022)

The best performance was achieved for the device incorporating the 90% SF-PDI$_2$ accepter. This device exhibited an approximately 22% increase in J_{SC} compared to the device with the 100% SF-PDI$_2$ acceptor, indicating that m-PDI-induced aggregation enhances photocurrent generation [41–43]. Further increasing the m-PDI content led to a deterioration in device performance. Specifically, the device containing the 80% SF-PDI$_2$ acceptor showed lower J_{SC} and PCE values than the device with the 100% SF-PDI$_2$ acceptor. This performance degradation at m-PDI content exceeding the optimal level is likely attributable to excessive acceptor aggregation induced by m-PDI. Meanwhile, the device based on the 0% SF-PDI$_2$ acceptor, corresponding to 100% m-PDI, exhibited substantially reduced J_{SC}, V_{OC}, and PCE values, confirming that excessive aggregation of m-PDI is detrimental to device performance.

The EQE spectra of the devices are shown in Figure 4b. The spectral profiles of the EQE spectra closely follow those of the UV-vis absorption spectra. The device incorporating 90% SF-PDI$_2$ exhibits the highest EQE values, reaching up to approximately 18% across the visible range, followed by devices with 100% SF-PDI$_2$, 80% SF-PDI$_2$, and 0% SF-PDI$_2$ acceptors. This trend is in good agreement with the J_{SC} values extracted from the *J*-*V* measurements.

Overall, the photovoltaic characteristics shown in Figure 4 demonstrate that moderate PDI aggregation in the 90% SF-PDI$_2$ blend effectively facilitates efficient photocurrent generation, consistent with our hypothesis. Devices based on 100% SF-PDI$_2$ exhibit slightly lower J_{SC} and EQE values, likely because the absence of aggregation limits the formation of efficient electron transport pathways. In contrast, devices containing 80% or less SF-PDI$_2$ show significant reductions in EQE as a result of excessive m-PDI aggregation, which disrupts the optimal donor–acceptor interpenetrating network.

To support our interpretation, electron-only SCLC measurements were performed on mixed-PDI-only films (Figure 5). The electron mobilities were extracted by fitting the SCLC *J*-*V* characteristics using Mott-Gurney law [44,45]. The extracted electron mobility values were 1.86×10^{-4}, 3.87×10^{-4}, 4.15×10^{-4}, and 1.28×10^{-3} cm^2 V^{-1} s^{-1} for the films containing 100% SF-PDI$_2$, 90% SF-PDI$_2$, 80% SF-PDI$_2$, and 0% SF-PDI$_2$ acceptors, respectively. The approximately twofold enhancement in electron mobility observed for the 90% SF-PDI$_2$ film compared to the 100% SF-PDI$_2$ film clearly demonstrates that the introduction of a small amount of m-PDI indeed facilitates electron transport within the PDI acceptor phase through controlled aggregation. Meanwhile, because m-PDI and SF-PDI$_2$ have comparable LUMO energy levels, their mixing is unlikely to substantially alter the energy landscape of the acceptor phase. This enhanced electron transport contributes directly to the improved performance of OSC devices based on the 90% SF-PDI$_2$ acceptor. In contrast, the similar electron mobility values obtained for the 90% SF-PDI$_2$ and 80% SF-PDI$_2$ films indicate that further increasing the m-PDI content does not lead to a continuous improvement in electron transport within the mixed PDI acceptor system.

Taken together, the results from UV-vis absorption, EQE, morphology, and charge transport analyses demonstrate that the complementary molecular structures of m-PDI and SF-PDI$_2$ enable fine tuning of aggregation behavior and film morphology in the photoactive layer. This synergistic effect leads to enhanced overall photovoltaic performance in mixed-acceptor devices when the blending ratio between the complementary acceptors is optimally controlled.

Finally, we note that the PCEs of the devices reported in this study are lower than those reported in some PDI-based OSC literature demonstrating high PCE values. Device performance could be further improved through various approaches, such as changing the donor polymer, adjusting the donor to acceptor ratio, introducing solvent additives to control the nanoscale morphology, or employing alternative interlayer materials. However,

the primary objective of this study is not to achieve record high PCE, but rather to validate the concept of mixing PDI acceptors with complementary molecular structures and to elucidate its effect on aggregation behavior and morphology. Therefore, we deliberately employed an experimental system that allows the effects of mixing two PDI acceptors to be clearly and unambiguously observed, even at the expense of device PCEs. As evidenced by the consistent trends across multiple datasets, our results demonstrate the reliability of our experimental observations and confirm the effectiveness of the mixed-PDI acceptor strategy.

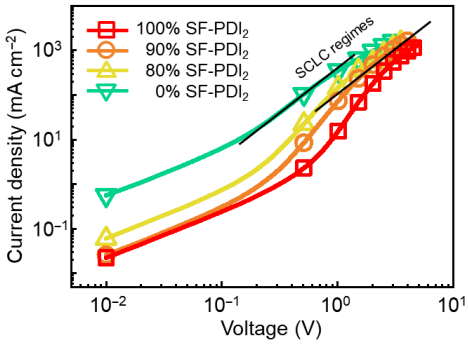

Figure 5. Electron-only SCLC characteristics of mixed-PDI-only devices. The thickness of the mixed-PDI layers was ~35 nm for all samples.

4. Conclusions

In summary, this study demonstrates a mixed-acceptor strategy that combines planar and twisted PDI acceptors as an effective approach to control molecular aggregation behavior and optimize photoactive layer morphology in OSCs. The motivation of this work arises from the intrinsic trade-off in PDI-based acceptors, where strong aggregation of planar molecular structures leads to excessive aggregation of PDI molecules and pronounced phase separation between the donor and acceptor, whereas highly twisted molecular structures suppress excessive phase separation but can limit efficient electron transport. By blending m-PDI and SF-PDI$_2$, two acceptors with complementary molecular geometries, we aimed to balance these opposing effects within a single photoactive layer. Systematic variation in the acceptor composition revealed that introducing a small amount of planar m-PDI into an amorphous SF-PDI$_2$-rich matrix induces controlled and moderate aggregation without causing severe crystallization or phase separation. Spectroscopic and morphological analyses confirmed that this subtle aggregation enhances molecular packing while preserving overall film uniformity. As a result, devices incorporating the optimized mixed-acceptor composition exhibited improved photocurrent generation and EQE compared to devices based on a single acceptor system. The best photovoltaic performance was achieved for the blend containing 90% SF-PDI$_2$, which showed a clear enhancement in J_{SC} and PCE. Electron-only transport measurements further revealed that this improvement originates from enhanced electron mobility enabled by controlled aggregation in the acceptor phase. In contrast, higher m-PDI contents led to excessive aggregation and degraded device performance, emphasizing that aggregation must be precisely tuned.

Overall, this work establishes acceptor blending with complementary aggregation behavior as a simple and versatile strategy to engineer molecular aggregation in OSCs without the need for complex molecular redesign. We believe this concept can be readily extended to other non-fullerene acceptor systems that face similar structure–property trade-offs.

Author Contributions: Conceptualization, H.L.; Methodology, H.L.; Data Curation, H.H. and H.L.; Formal Analysis, H.H. and H.L.; Writing—Original Draft Preparation, H.H. and H.L.; Writing—Review and Editing, H.H. and H.L.; Visualization, H.H. and H.L.; Funding Acquisition, H.L. All authors have read and agreed to the published version of the manuscript.

Funding: This work was supported by the Gachon University research fund of 2024 (GCU-202500890001).

Data Availability Statement: The original contributions presented in the study are included in the article. Further inquiries can be directed to the corresponding authors.

Conflicts of Interest: The authors declare no conflicts of interest.

References

1. Zhang, X.; Lu, Z.; Ye, L.; Zhan, C.; Hou, J.; Zhang, S.; Jiang, B.; Zhao, Y.; Huang, J.; Zhang, S.; et al. A Potential Perylene Diimide Dimer-Based Acceptor Material for Highly Efficient Solution-Processed Non-Fullerene Organic Solar Cells with 4.03% Efficiency. *Adv. Mater.* **2013**, *25*, 5791–5797. [CrossRef]
2. Lee, H.; Park, C.; Sin, D.H.; Park, J.H.; Cho, K. Recent Advances in Morphology Optimization for Organic Photovoltaics. *Adv. Mater.* **2018**, *30*, 1800453. [CrossRef]
3. Cusumano, P.; Arnone, C.; Giambra, M.A.; Parisi, A. Donor/Acceptor Heterojunction Organic Solar Cells. *Electronics* **2020**, *9*, 70. [CrossRef]
4. Kesava, S.V.; Fei, Z.; Rimshaw, A.D.; Wang, C.; Hexemer, A.; Asbury, J.B.; Heeney, M.; Gomez, E.D. Domain Compositions and Fullerene Aggregation Govern Charge Photogeneration in Polymer/Fullerene Solar Cells. *Adv. Energy Mater.* **2014**, *4*, 1400116. [PubMed]
5. Schubert, M.; Dolfen, D.; Frisch, J.; Roland, S.; Steyrleuthner, R.; Stiller, B.; Chen, Z.; Scherf, U.; Koch, N.; Facchetti, A.; et al. Influence of Aggregation on the Performance of All-Polymer Solar Cells Containing Low-Bandgap Naphthalenediimide Copolymers. *Adv. Energy Mater.* **2012**, *2*, 369–380. [CrossRef]
6. Kwon, O.K.; Park, J.H.; Park, S.K.; Park, S.Y. Soluble Dicyanodistyrylbenzene-Based Non-Fullerene Electron Acceptors with Optimized Aggregation Behavior for High-Efficiency Organic Solar Cells. *Adv. Energy Mater.* **2014**, *5*, 1400929. [CrossRef]
7. Ye, L.; Sun, K.; Jiang, W.; Zhang, S.; Zhao, W.; Yao, H.; Wang, Z.; Hou, J. Enhanced Efficiency in Fullerene-Free Polymer Solar Cell by Incorporating Fine-Designed Donor and Acceptor Materials. *ACS Appl. Mater. Interfaces* **2015**, *7*, 9274–9280. [CrossRef]
8. Yin, H.; Ma, L.K.; Wang, Y.; Huang, J.; Yu, H.; Zhang, J.; Chow, P.C.Y.; Ma, W.; So, S.K.; Yan, H. Donor Polymer Can Assist Electron Transport in Bulk Heterojunction Blends with Small Energetic Offsets. *Adv. Mater.* **2019**, *31*, e1903998. [CrossRef]
9. Akash; Tiwari, J.P. Recent Advancements in Perylene Diimide as an Electron Acceptor in Organic Solar Cells. *J. Mater. Chem. C* **2024**, *12*, 838–853. [CrossRef]
10. Eynaud, Q.; Koganezawa, T.; Sekimoto, H.; Kramdi, M.E.A.; Quéléver, G.; Margeat, O.; Ackermann, J.; Yoshimoto, N.; Videlot-Ackermann, C. Ternary Polymer Solar Cells: Impact of Non-Fullerene Acceptors on Optical and Morphological Properties. *Electronics* **2024**, *13*, 1752. [CrossRef]
11. Cooling, N.A.; Feron, K.; Jones, T.W.; Belcher, W.J.; Dastoor, P.C. Controlling Charge Generation in Organic Photovoltaic Ternary Blends: How Trace Ternary Additives Determine Mechanism. *Electronics* **2025**, *14*, 1655. [CrossRef]
12. Xu, W.; Tian, H.; Ni, Y.; Xu, Y.; Zhang, L.; Zhang, F.; Wu, S.; Young Jeong, S.; Huang, T.; Du, X.; et al. Eco-Friendly Solvent-Processed Layer-by-Layer Ternary All-Polymer Solar Cells Exhibiting over 18.5% Efficiency. *Chem. Eng. J.* **2024**, *493*, 152558. [CrossRef]
13. Zhang, C.; Sun, S.; Han, T.; Chi, J.; Dong, R.; Han, S.; Zhou, H.; Xu, Y.; Cai, L.; Du, X.; et al. Superior Charge Dynamics Via Ternary Doping Layer-by-Layer Strategy in High-Efficiency Organic Solar Cells. *Chem. Eng. J.* **2025**, *522*, 167959. [CrossRef]
14. Zhong, Y.; Trinh, M.T.; Chen, R.; Wang, W.; Khlyabich, P.P.; Kumar, B.; Xu, Q.; Nam, C.Y.; Sfeir, M.Y.; Black, C.; et al. Efficient Organic Solar Cells with Helical Perylene Diimide Electron Acceptors. *J. Am. Chem. Soc.* **2014**, *136*, 15215–15221. [CrossRef] [PubMed]
15. Wu, C.H.; Chueh, C.C.; Xi, Y.Y.; Zhong, H.L.; Gao, G.P.; Wang, Z.H.; Pozzo, L.D.; Wen, T.C.; Jen, A.K.Y. Influence of Molecular Geometry of Perylene Diimide Dimers and Polymers on Bulk Heterojunction Morphology toward High-Performance Nonfullerene Polymer Solar Cells. *Adv. Funct. Mater.* **2015**, *25*, 5326–5332. [CrossRef]
16. Lee, J.; Singh, R.; Sin, D.H.; Kim, H.G.; Song, K.C.; Cho, K. A Nonfullerene Small Molecule Acceptor with 3d Interlocking Geometry Enabling Efficient Organic Solar Cells. *Adv. Mater.* **2016**, *28*, 69–76. [CrossRef] [PubMed]
17. Cao, J.; Yang, S. Progress in Perylene Diimides for Organic Solar Cell Applications. *RSC Adv.* **2022**, *12*, 6966–6973. [CrossRef] [PubMed]
18. Cheng, P.; Zhao, X.; Zhan, X. Perylene Diimide-Based Oligomers and Polymers for Organic Optoelectronics. *Acc. Mater. Res.* **2022**, *3*, 309–318. [CrossRef]

19. Sugie, A.; Han, W.; Shioya, N.; Hasegawa, T.; Yoshida, H. Structure-Dependent Electron Affinities of Perylene Diimide-Based Acceptors. *J. Phys. Chem. C* **2020**, *124*, 9765–9773. [CrossRef]
20. Sun, J.-P.; Hendsbee, A.D.; Dobson, A.J.; Welch, G.C.; Hill, I.G. Perylene Diimide Based All Small-Molecule Organic Solar Cells: Impact of Branched-Alkyl Side Chains on Solubility, Photophysics, Self-Assembly, and Photovoltaic Parameters. *Org. Electron.* **2016**, *35*, 151–157. [CrossRef]
21. Qu, J.; Mu, Z.; Lai, H.; Xie, M.; Liu, L.; Lu, W.; Chen, W.; He, F. Effect of the Molecular Configuration of Perylene Diimide Acceptors on Charge Transfer and Device Performance. *ACS Appl. Energy Mater.* **2018**, *1*, 833–840. [CrossRef]
22. Singh, R.; Suranagi, S.R.; Lee, J.; Lee, H.; Kim, M.; Cho, K. Unraveling the Efficiency-Limiting Morphological Issues of the Perylene Diimide-Based Non-Fullerene Organic Solar Cells. *Sci. Rep.* **2018**, *8*, 2849. [CrossRef]
23. Lin, Y.; Wang, Y.; Wang, J.; Hou, J.; Li, Y.; Zhu, D.; Zhan, X. A Star-Shaped Perylene Diimide Electron Acceptor for High-Performance Organic Solar Cells. *Adv. Mater.* **2014**, *26*, 5137–5142. [CrossRef] [PubMed]
24. Zhao, D.; Wu, Q.; Cai, Z.; Zheng, T.; Chen, W.; Lu, J.; Yu, L. Electron Acceptors Based on A-Substituted Perylene Diimide (Pdi) for Organic Solar Cells. *Chem. Mater.* **2016**, *28*, 1139–1146. [CrossRef]
25. Liu, Z.; Zhang, L.; Shao, M.; Wu, Y.; Zeng, D.; Cai, X.; Duan, J.; Zhang, X.; Gao, X. Fine-Tuning the Quasi-3d Geometry: Enabling Efficient Nonfullerene Organic Solar Cells Based on Perylene Diimides. *ACS Appl. Mater. Interfaces* **2018**, *10*, 762–768. [CrossRef]
26. Wu, M.; Yi, J.P.; Chen, L.; He, G.; Chen, F.; Sfeir, M.Y.; Xia, J. Novel Star-Shaped Helical Perylene Diimide Electron Acceptors for Efficient Additive-Free Nonfullerene Organic Solar Cells. *ACS Appl. Mater. Interfaces* **2018**, *10*, 27894–27901. [CrossRef]
27. Luo, Z.; Liu, T.; Chen, Z.; Xiao, Y.; Zhang, G.; Huo, L.; Zhong, C.; Lu, X.; Yan, H.; Sun, Y.; et al. Isomerization of Perylene Diimide Based Acceptors Enabling High-Performance Nonfullerene Organic Solar Cells with Excellent Fill Factor. *Adv. Sci.* **2019**, *6*, 1802065. [CrossRef] [PubMed]
28. Ding, K.; Wang, Y.; Shan, T.; Xu, J.; Bao, Q.; Liu, F.; Zhong, H. Propeller-Like Acceptors with Difluoride Perylene Diimides for Organic Solar Cells. *Org. Electron.* **2020**, *78*, 105569. [CrossRef]
29. Liu, W.; Zhang, C.; Liu, J.; Bo, Z. Pdi-Based Hexapod-Shaped Nonfullerene Acceptors for the High-Performance as-Cast Organic Solar Cells. *ACS Appl. Mater. Interfaces* **2020**, *12*, 37409–37417. [CrossRef]
30. Li, Z.; Li, D.; Bao, Y.; Guo, P.; Liang, Z.; Yang, C.; Tong, J. Acceptor-Acceptor Type Perylenediimide-Based Polymeric Acceptors with Large 2-Decyltetradecyl Flexible Side Chain: Synthesis and Impact of Fluorination. *Opt. Mater.* **2025**, *162*, 116932. [CrossRef]
31. Song, K.C.; Singh, R.; Lee, J.; Sin, D.H.; Lee, H.; Cho, K. Propeller-Shaped Small Molecule Acceptors Containing a 9,9′-Spirobifluorene Core with Imide-Linked Perylene Diimides for Non-Fullerene Organic Solar Cells. *J. Mater. Chem. C* **2016**, *4*, 10610–10615. [CrossRef]
32. Singh, R.; Lee, J.; Kim, M.; Keivanidis, P.E.; Cho, K. Control of the Molecular Geometry and Nanoscale Morphology in Perylene Diimide Based Bulk Heterojunctions Enables an Efficient Non-Fullerene Organic Solar Cell. *J. Mater. Chem. A* **2017**, *5*, 210–220. [CrossRef]
33. Chen, R.; Wang, H.; Yuan, S.; Jia, T.; Luo, Y.; Lin, T.; Xu, Y.; Li, Q.; Li, Y.; Xiao, B.; et al. Modulated Aggregation on Terpolymer Towards 19.2% Green Solvent Processed Binary Organic Solar Cells. *Nano Energy* **2025**, *134*, 110576. [CrossRef]
34. Weng, K.; Li, C.; Bi, P.; Ryu, H.S.; Guo, Y.; Hao, X.; Zhao, D.; Li, W.; Woo, H.Y.; Sun, Y. Ternary Organic Solar Cells Based on Two Compatible Pdi-Based Acceptors with an Enhanced Power Conversion Efficiency. *J. Mater. Chem. A* **2019**, *7*, 3552–3557. [CrossRef]
35. Lu, H.; Liu, J.; Liu, Y.; Xu, X.; Bo, Z. Improving the Efficiency of Organic Solar Cells by Introducing Perylene Diimide Derivative as Third Component and Individually Dissolving Donor/Acceptor. *ChemSusChem* **2021**, *14*, 5442–5449. [CrossRef]
36. Liu, M.; Ge, X.; Jiang, X.; Chen, D.; Guo, F.; Gao, S.; Peng, Q.; Zhao, L.; Zhang, Y. 18% Efficiency of Ternary Organic Solar Cells Enabled by Integrating a Fused Perylene Diimide Guest Acceptor. *Nano Energy* **2023**, *112*, 108501. [CrossRef]
37. Lee, H.; Lee, D.; Sin, D.H.; Kim, S.W.; Jeong, M.S.; Cho, K. Effect of Donor–Acceptor Molecular Orientation on Charge Photogeneration in Organic Solar Cells. *npg Asia Mater.* **2018**, *10*, 469–481. [CrossRef]
38. Farahat, M.E.; Welch, G.C. N-Annulated Perylene Diimide Non-Fullerene Acceptors for Organic Photovoltaics. *Colorants* **2023**, *2*, 151–178. [CrossRef]
39. An, Q.; Wang, J.; Gao, W.; Ma, X.; Hu, Z.; Gao, J.; Xu, C.; Hao, M.; Zhang, X.; Yang, C.; et al. Alloy-Like Ternary Polymer Solar Cells with over 17.2% Efficiency. *Sci. Bull.* **2020**, *65*, 538–545. [CrossRef]
40. Naqvi, S.; Kumar, M.; Kumar, R. Facile Synthesis and Evaluation of Electron Transport and Photophysical Properties of Photoluminescent Pdi Derivatives. *ACS Omega* **2019**, *4*, 19735–19745. [CrossRef] [PubMed]
41. Fang, J.; Wang, Z.; Chen, Y.; Zhang, Q.; Zhang, J.; Zhu, L.; Zhang, M.; Cui, Z.; Wei, Z.; Ade, H.; et al. Revealing Aggregation of Non-Fullerene Acceptors in Intermixed Phase by Ultraviolet-Visible Absorption Spectroscopy. *Cell Rep. Phys. Sci.* **2022**, *3*, 100983. [CrossRef]
42. Guo, C.; Fu, Y.; Li, D.; Wang, L.; Zhou, B.; Chen, C.; Zhou, J.; Sun, Y.; Gan, Z.; Liu, D.; et al. A Polycrystalline Polymer Donor as Pre-Aggregate toward Ordered Molecular Aggregation for 19.3% Efficiency Binary Organic Solar Cells. *Adv. Mater.* **2023**, *35*, e2304921. [CrossRef] [PubMed]

43. Zhang, J.; Zhong, J.; Chung, S.; Bai, L.; Zhao, Z.; Tan, L.; Liu, Y.; Zhang, M.; Lyu, S.; Lee, J.; et al. Π-Conjugation-Driven Aggregation Enhances Charge Transport in Y6 Derivatives for Bilayer Organic Solar Cells with 20 % Efficiency. *Chem. Eng. J.* **2025**, *522*, 167311. [CrossRef]
44. Montero, J.M.; Bisquert, J. Interpretation of Trap-Limited Mobility in Space-Charge Limited Current in Organic Layers with Exponential Density of Traps. *J. Appl. Phys.* **2011**, *110*, 043705. [CrossRef]
45. Nicolai, H.T.; Mandoc, M.M.; Blom, P.W.M. Electron Traps in Semiconducting Polymers: Exponential Versus Gaussian Trap Distribution. *Phys. Rev. B* **2011**, *83*, 195204. [CrossRef]

Disclaimer/Publisher's Note: The statements, opinions and data contained in all publications are solely those of the individual author(s) and contributor(s) and not of MDPI and/or the editor(s). MDPI and/or the editor(s) disclaim responsibility for any injury to people or property resulting from any ideas, methods, instructions or products referred to in the content.